2021-01-1157 Published 21 Sep 2021



Spark Ignition Discharge Characteristics under Quiescent Conditions and with Convective Flows

Corey Tambasco Univ of Texas-Austin

Delong Li Univ. of Texas at Ausitn

Matthew Hall Univ. of Texas-Austin

Ronald Matthews Univ of Texas-Austin

Citation: Tambasco, C., Li, D., Hall, M., and Matthews, R., "Spark Ignition Discharge Characteristics under Quiescent Conditions and with Convective Flows," SAE Technical Paper 2021-01-1157, 2021, doi:10.4271/2021-01-1157.

Abstract

he arc characteristics and discharge behavior of a representative inductive spark ignition system were characterized with a spark plug calorimeter and a constant volume vessel used to create high-pressure crossflow velocities through the gap of the spark plug. A 14 mm diameter natural gas engine spark plug was used for the measurements. The discharges were into a non-combusting gas, primarily nitrogen.

The spark plug calorimeter was used to determine the electrical-to-thermal energy conversion in the spark gap under quiescent conditions, while the constant volume vessel was used to study ignition arc structure in convective crossflows and imaged with a high-speed camera. Topics included the effect of crossflow velocity, pressure (up to 20 bar at 300 K), and gap distance on breakdown voltage, arc duration and delivered electrical energy. Also of interest was the

amount of remaining electrical energy on the coil versus spark duration in a cross flow. Resistance of the arc plasma during the discharge was correlated with arc length and the delivered electrical energy was compared with that dissipated in the internal resistance of the spark plug. The relationship between arc stretch and arc width was studied, as well. The post-breakdown arc voltage and current were correlated with images of the convected plasma arc to elucidate features associated with short-circuiting and restrikes. The relationships among spark duration, arc length and gap flow velocity were also considered. An interesting finding was that the shortened spark duration under high crossflow velocity was due to the more rapid depletion of the electrical energy stored in the secondary side of the inductive ignition circuit rather than to arc instabilities associated with the disturbance of the arc by the flow.

Introduction

he discharge characteristics of an inductive spark ignition system were studied in quiescent conditions and with varying crossflow velocities through the gap. Under quiescent conditions the current, gap-voltage, and electrical and thermal energy deposition in the gap were measured using a spark plug calorimeter for a range of pressures and spark gap distances.

Simulations of the arc size and shape for quiescent conditions were conducted with the *VizSpark* (Esgee Technologies, Inc.) multi-dimensional spark simulation code to compare against experimental values of breakdown and follow-on voltages, current, and arc size and shape. Of particular interest was the predicted arc width (diameter) which may be important for arc to electrode heat transfer and for comparison with the measured diameter of the convected arc under crossflow conditions

The details of the spark ignition process are important to early flame kernel development. Newer generation engines, and natural gas engines in particular, are being pushed toward higher bmeps and using more dilution for emissions control. These factors have added to the challenges of ensuring successful and reliable spark ignition. Many prior studies have examined the details of the spark ignition process. Pashley et al. [1] used voltage and current traces to present new correlations for breakdown voltage as a function of gap distance, gas composition, temperature, and pressure. As is well known, they found that increased pressure resulted in higher breakdown voltages due to the increased density of the gas. They concluded that this effect reduced the amount of energy available for the glow discharge regime, shortening spark duration. They also looked at spark discharges in pressurized flow fields, from which they found that spark durations could be shortened by up to 75% due to stretching of the arc at a flow velocity of 25 m/s.

Shiraishi et al. [2] looked at effects of pressure, flow velocity, and current trace characteristics using a constant volume combustion chamber, four different ignition coils, and with a single cylinder engine. They focused on arc stretching and restrike events during the discharge process. Spark channel

length was found to increase at higher pressures (above 500 kPa) and with high flow velocities, while the time to the first restrike event decreased. Inversely, at lower pressures, they found the stretched length of the arc did not follow the flow velocity closely, the spark length shortened, and the time to the first restrike increased. However, crossflow velocity was limited to 7.9 m/s.

Yang et al. [3] investigated connecting an external capacitor in parallel with a spark plug to increase the discharge energy during breakdown. This was done because the electrical-to-thermal energy transfer efficiency is known to be greatest during the breakdown regime [4]. Various parallel capacitance levels (up to 500 pF) were tested at pressures up to 7 bar and flow velocities of 15 m/s. Parallel capacitance was found to redistribute the energy to the spark plug by taking energy from the glow phase of the discharge and supplying it to the breakdown phase. This was achieved by increasing breakdown duration, rather than breakdown voltage, which in turn decreases total discharge duration. They also found that this method helped promote flame kernel formation in quiescent conditions but lost its effect under flow conditions.

Zadeh et al. [5] used a constant volume optical combustion-vessel to look at arc stretch in flow conditions with velocities up to 32 m/s. They considered pressures from 15 to 45 bar as well as gap sizes of 0.30 mm and 0.65 mm. They found that restrikes occur with higher frequency at greater flow velocities due to the increasing discharge energy, as the voltage across the stretched arc exceeds the minimum voltage required to form a new arc between the spark plug electrodes. They also found that discharge duration decreases with increasing gas pressure, while the corresponding discharge energy increases with flow velocity but decreases with increasing gas pressure.

Huang et al. [6] also used optical imaging techniques to look at the restrike and short circuit characteristics of a spark plug in crossflow, considering relatively large gap sizes of 1 mm to 3 mm and flow velocities of 50 to 150 m/s. They found that the restrike voltage is lower than the breakdown voltage from the same discharge process. They also saw that the growth rate is not dependent on the discharge energy or spark plug gap size but is approximately twice the crossflow velocity. However, all their measurements were conducted at atmospheric pressure.

Abidin et al. [7] performed experiments using a spark calorimeter to characterize the spark discharge based on the parameters of pressure, gap size, and supplied primary energy. They considered pressures of 5 to 9 bar and gap sizes of 0.8 to 1.5 mm, all under quiescent conditions. These parameters were varied to determine their impact on breakdown voltage, secondary energy, energy delivered to the gas, energy conversion efficiency, and spark duration. They found that conversion efficiency increased, and spark duration decreased with an increase in either pressure or gap size. They also found that, for a pressure of 9 bar, gap size of 0.8 mm, and dwell time of 0.5 ms, approximately half of the energy on the secondary side of the circuit was lost to the spark plug resistance, while the other half was delivered to the spark plug gap. Lakshmipathi et al. [8] also studied aspects of the electrical energy delivery for a spark plug considering spark plug capacitance and internal resistance. They found that electrical energy delivery to the gap increased with both spark gap size and pressure, looking at gap sizes from 0.5 to 2.0 mm but pressures from only 1 to 4 bar.

In one of our prior studies, Kim et al. [9] used a spark plug calorimeter to study the electrical-to-thermal energy conversion in the spark gap for arc discharges over a range of pressures up to 24 bar and for different gap distances and dwell times.

The current study differs from those in the past in several ways. Firstly, the study used a 14 mm J-gap spark plug designed for natural gas engines. The spark plug had an internal resistance of 4.55 kOhm. The calorimeter measurements were used to establish baseline performance under quiescent conditions for comparison with measurements of arc geometry and electrical energy delivery and utilization under high-pressure crossflow conditions. The simulations were used to predict the arc diameter under quiescent conditions, which can be difficult to resolve experimentally within a very small gap and where the brightness of the arc can tend to saturate the camera images, particularly at higher pressures. They could then be compared with convected arc images that are more easily resolved experimentally.

Calorimeter

This study used the same calorimeter as that used by Kim et al. [9], except that the original pressure sensor was replaced with one having better time resolution. The setup used for these experiments was described in previous papers [9, 10, 11], but is summarized here for completeness. First, calorimeter measurements were made to determine the conversion efficiency of electrical energy delivered to the spark plug gap to thermal energy deposited in the gas. A schematic of the calorimeter setup is shown in Figure 1. The calorimeter was machined from stainless steel to house a 14 mm spark plug. The calorimeter was designed with two chambers to allow the differential pressure rise from the spark to be measured. Two valves separate the two chambers from each other and admit the outside gas. Between the two valves was a piezoresistive pressure transducer (Endevco 8510B-2) rated for differential

FIGURE 1 Schematic of calorimeter setup.

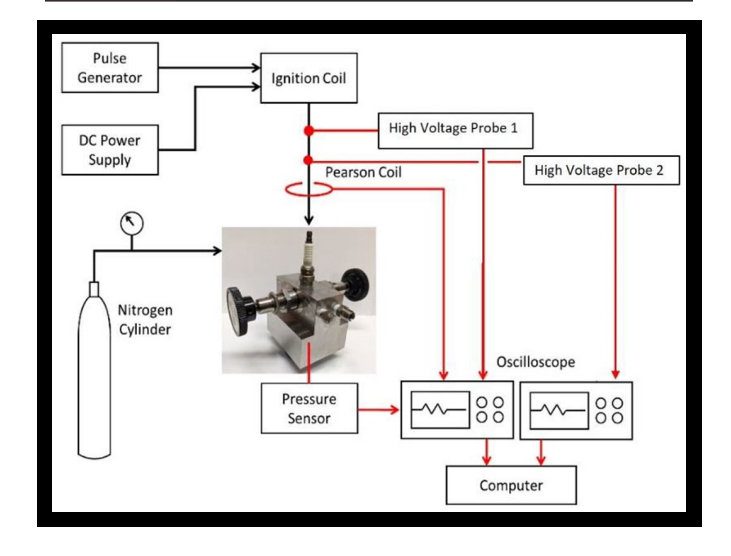
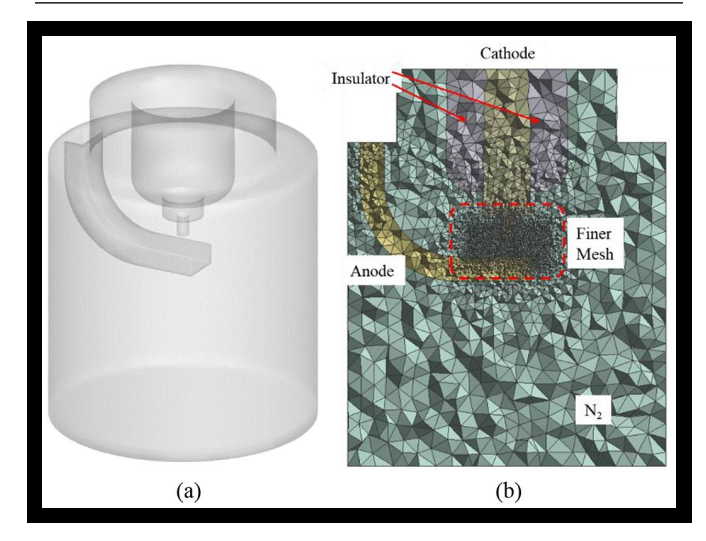


FIGURE 2 VizSpark CFD computational domain (a) and simulation mesh of the spark plug and calorimeter volume (b)



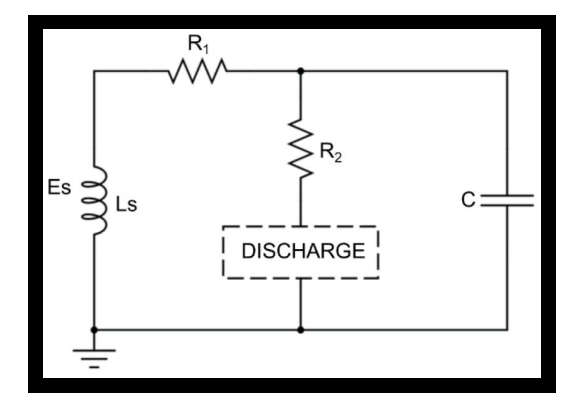
pressures up to 2 psig (13.8 kPa). This allowed us to measure the small pressure rises created in the top chamber by the energy deposition of the spark.

Nitrogen was used to pressurize the calorimeter to pressures up to 20 bar, measured using precision Bourdon tube pressure gauges. Two separate high voltage probes (Tektronix Model P6015A) were connected to the ignition coil to make time-resolved measurements of voltage at the top of the spark plug. One of the probes connected to a Siglent 100 MHz dualchannel oscilloscope with a finer time resolution (10 ns) for measuring breakdown voltages. The other probe connected to a Tektronix 100 MHz 4-channel oscilloscope with a slower time resolution setting (320 ns) which was used for measuring voltage over the entire spark discharge. This oscilloscope also recorded the trace from the pressure transducer and a Pearson Model 110 current sensor for measuring current over the spark discharge. The current-dependent resistance of the spark plug was measured prior to beginning the experiments and the voltage drop across the resistor was subtracted from the measured voltages to obtain gap voltage values.

Simulations

The calorimeter experimental results were compared with multi-dimensional simulations. A thermal plasma modeling solver, *VizSpark*, was utilized for all of the simulations shown in this paper. *VizSpark* was developed by Esgee Technologies and has previously demonstrated high fidelity for modelling arc formation, stretch, and re-strike phenomena in the gap of a spark plug [12, 13]. It models fluid flow physics, electromagnetic phenomena, and chemical kinetics by solving a coupled set of governing equations simultaneously, including the Navier-Stokes equations, electromagnetic equations, and finite-rate chemistry equations. Depending on the complexity of a problem, different combinations of equations can be selected to address different kinds of problems. *VizSpark* is fully parallelized and thus fully qualified to three-dimensional simulations with complex geometries. More details

FIGURE 3 Secondary circuit used in the simulations



about the solver can be found by referring to these papers [12, 13]. For this study, neither chemical kinetics nor surface ablation was simulated, and each case was solved in about 5-6 days by using 48 processors in parallel.

The three-dimensional calorimeter volume dimensions were meshed for the simulations. The spark plug had a cathode diameter of 0.6 mm and a 0.63 mm gap, the same as the experiments and shown in Figure 2a. The mesh at the middle cutplane is shown in Figure 2b. The entire domain was meshed by using tetrahedral elements; there were about 0.44 million cells in total. Local refinement to 75-micrometer cell size was performed in the spark plug gap region to resolve the high property gradients across the arc, and the maximum cell size was limited to 0.7 mm for the rest of the calculation domain. Local refinement to 75-micrometer cell size was performed in the spark plug gap region to resolve the high property gradients across the arc. The calorimeter was filled with nitrogen at a temperature of 300 K with no initial velocity and the initial pressure was changed in different cases ranging from 1 to 30 bar for comparison with the experiments. For the electromagnetic equations, all of the boundaries other than the cathode top surface were assigned a Dirichlet boundary condition with a zero potential. There is no turbulence model in *VizSpark* so any induced flows caused by the arc expansion would be modeled as laminar, consequently, there is no turbulent dispersion affecting the arc shape in the simulations.

An electric circuit on the secondary side, shown in Figure 3, was connected to the cathode (center electrode) top surface to model the discharge process more realistically. The resistances (R_1, R_2) , capacitance (C) and inductance (Ls) in the circuit came from the secondary side of the coil and the spark plug used in the experiments. The initial secondary coil energy (Es) was a function of the dwell time (120 mJ) for a 4 ms dwell time).

First, the breakdown voltages predicted by the simulations were compared with experimental results (<u>Figure 4</u>). The simulated breakdown voltages were very close to the measured ones within the pressure range of interest. Especially in the middle pressure range (10 bar, 15 bar), the values were within the experimental standard deviations (as indicated by the error bars) or very close.

The voltage and current traces at 20 bar are shown in <u>Figure 5a</u>. Three experimental traces are shown, for which the blue and green curves agreed so well that they mostly overlapped each other. The initial follow-on (post breakdown)

FIGURE 4 Breakdown voltages for the same spark plug at different pressures (nitrogen, 4 ms dwell time)

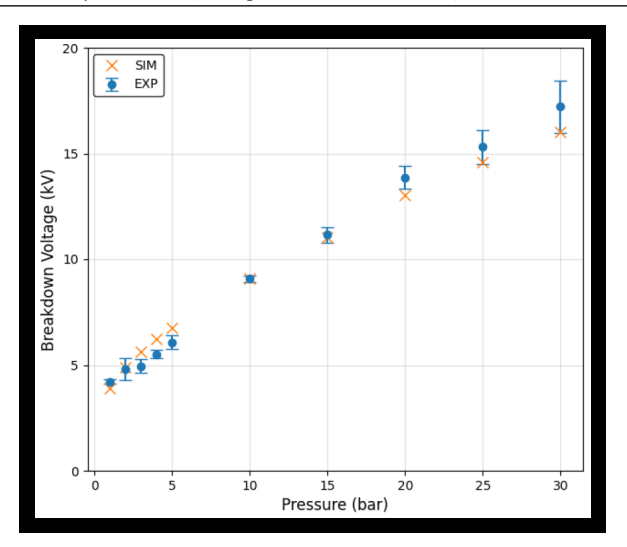
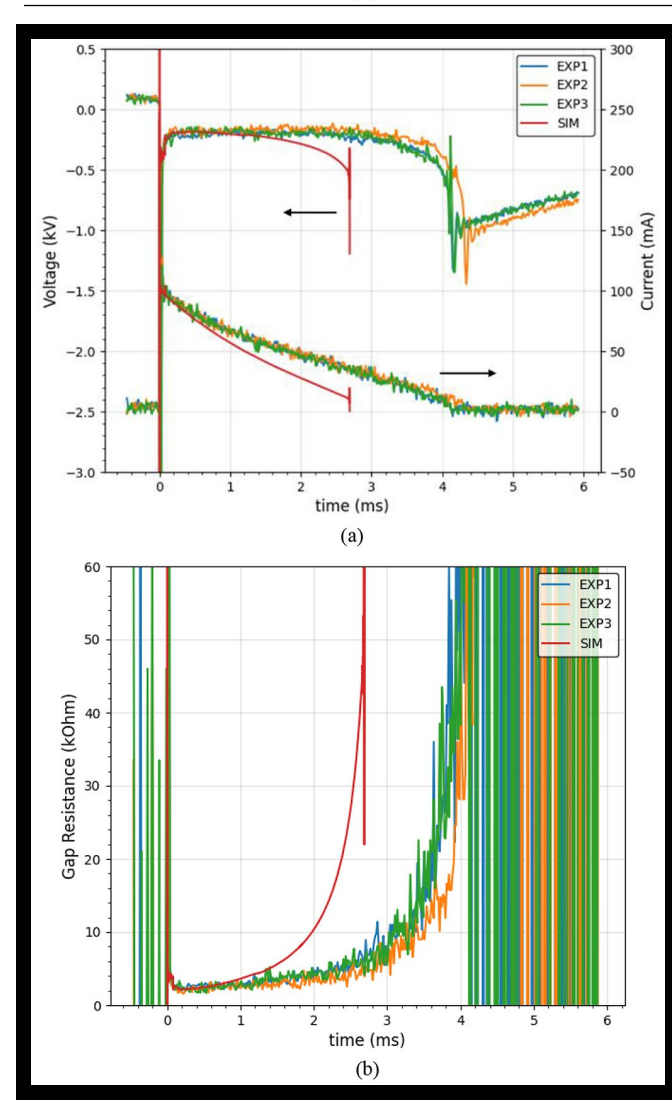


FIGURE 5 Voltage and current traces at 20 bar comparing three experimental traces (green, blue, and orange) with simulations (red) at a pressure of 20 bar, (a) Gap resistance, measured and from simulation, (b)



voltage and current predicted in the simulation matched the experiments reasonably well, but both decreased faster than the experimental values as the discharge progressed. Thus, the discharge time was less than 3 ms in the simulation, shorter than the 4.2 ms measured in the experiments. The discrepancy came from the inaccurate prediction of gap resistance, shown in Figure 5b. The initial predicted resistance, right after breakdown, again matched quite well with the experiments but increased more quickly than the experimental values. More work will be done together with Esgee Technologies to improve the follow-on gap resistance predictions.

Calorimeter Results

The next few figures show experimental results quantifying the electrical discharge characteristics measured in the calorimeter for quiescent conditions. Figure 6 shows the follow-on voltage following breakdown for different gap distances as a function of pressure. The discharges were almost entirely glow-type at 1 bar and almost entirely arc-type at 4 bar and above. The follow-on voltages increased with gap distance and weakly increased with increasing pressure. The gap voltages are important, as the electrical energy delivered to the gap is proportional to the gap voltage. The trends are consistent with increases in gap resistance with both gap distance and pressure.

Figure 7 shows the spark duration as a function of gap distance over the range of pressure investigated. There is a consistent trend of reduced spark duration as the gap distance increases and it also tends to decrease as pressure increases. A discussion of the physical processes leading to these trends is presented later.

<u>Figure 8</u> shows the electrical energy delivered to the gap as a function of gap distance. This trend is largely the opposite of spark duration; delivered electrical energy increases with gap distance. The delivered electrical energy tended to increase with increasing pressure, except for the glow-type discharges

FIGURE 6 Arc/glow voltage vs. pressure for three spark gaps

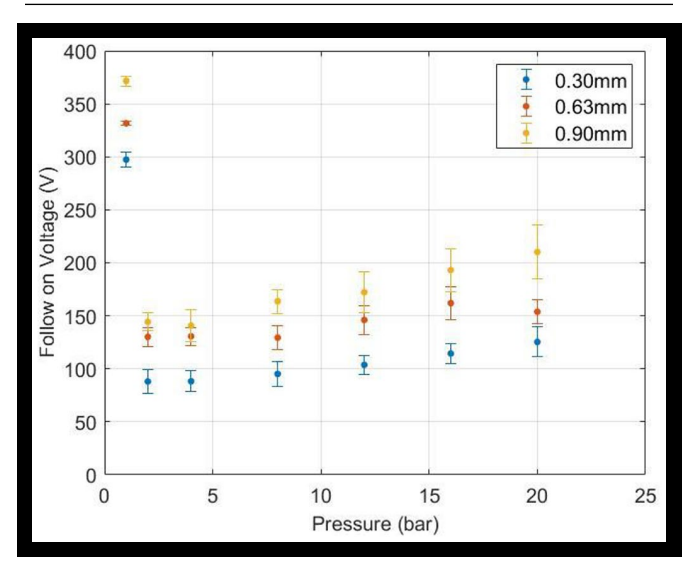


FIGURE 7 Spark duration vs. gap distance for a range of pressures

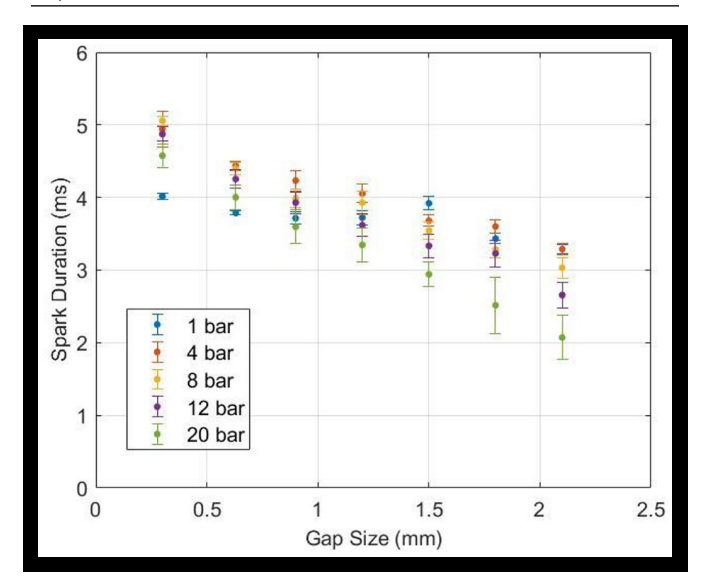
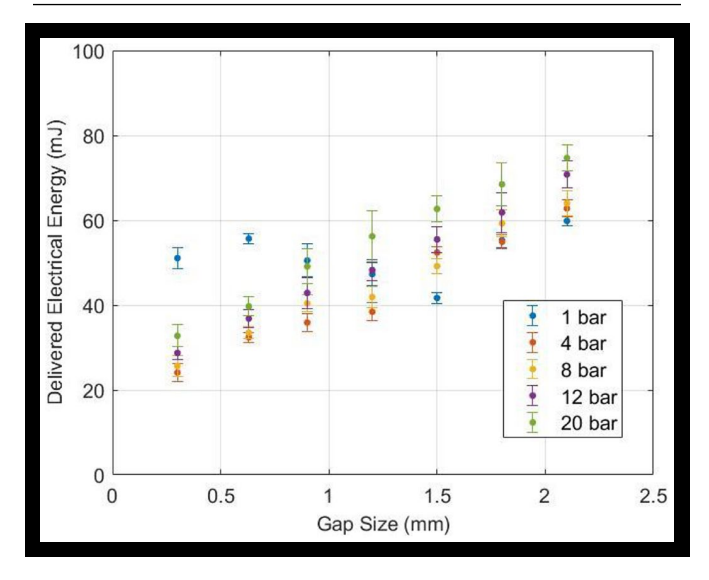


FIGURE 8 Electrical energy delivered to the gap vs. gap distance for a range of pressures



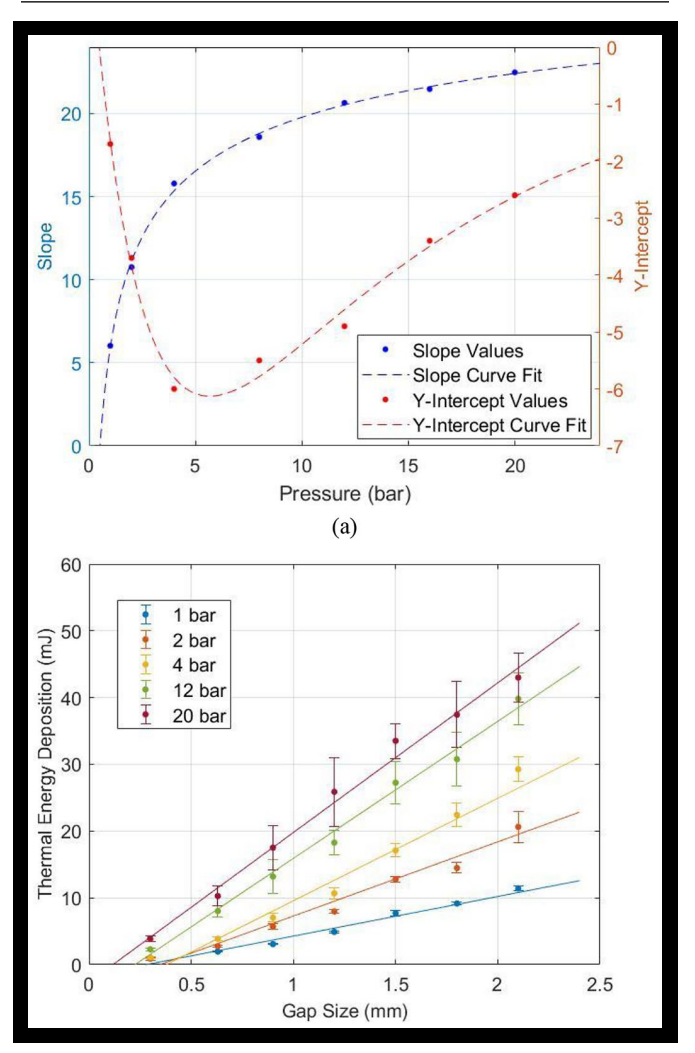
at low pressure, which had greater delivered electrical energy due to their high follow-on voltages. These trends are later seen to influence the energy budget and partitioning of the energy distribution.

From the measured pressure rise in the calorimeter, the thermal energy deposition to the nitrogen was determined (<u>Fig. 9</u>). The thermal energy deposition to the gas inside the calorimeter chamber was determined from the measured pressure rise using <u>Equation (1)</u>

$$E_{therm} = \frac{V}{\gamma - 1} \Delta P \tag{1}$$

In Equation (1), V is the chamber volume, ΔP is the maximum pressure rise and γ is the ratio of specific heats of nitrogen. Using this thermal energy deposition value, the conversion efficiency of electrical to thermal energy was found

FIGURE 9 Slope and Y intercept for linear curve fits of thermal energy, (a), Thermal energy delivered to the gas in the calorimeter vs. gap distance for various pressures.



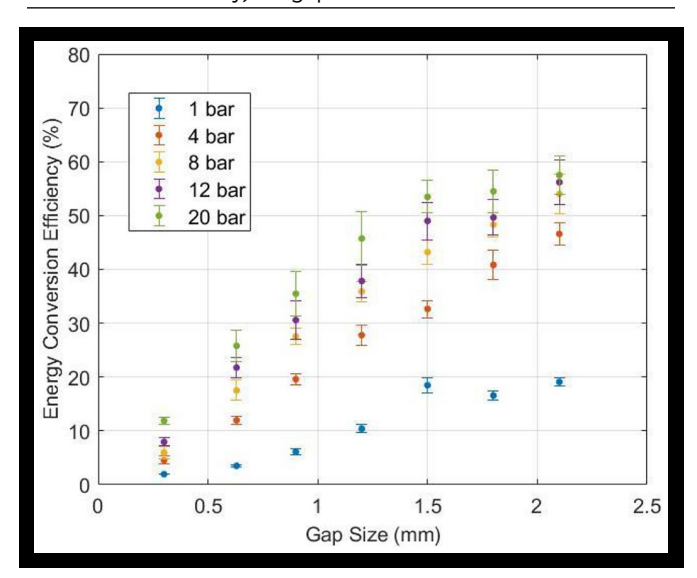
by dividing this value by the electrical energy supplied to the gap. The delivered electrical energy to the gap was determined as the integral of the measured current and voltage following the breakdown event and then subtracting the electrical energy dissipated in the spark plug resistor. Details of these measurements can be found in [9].

The portion of the electrical energy delivered to the gap that does not increase the thermal energy of the gas is lost to heat transfer [11]. The thermal energy deposition was found to be linear with gap distance and could be represented by a correlation (Equation 2) presented below as a function of both gap distance and pressure. Figure 9a shows the behavior the slope and Y-intercept values as a function of pressure. The slope behavior shows that the thermal energy deposition increases rapidly with pressure going from low to moderate pressures and while it continues to increase with pressure the rate of rise shows it to become less sensitive to further pressure increases.

The empirical expression derived for the thermal energy deposition as a function of pressure and gap distance is given by Equation 2.

$$E_{therm} = f_1(P)d_\sigma + f_2(P) \tag{2}$$

FIGURE 10 Thermal energy deposition to the gas divided by the electrical energy delivered to the gap (energy conversion efficiency) vs. gap distance.



where:

$$f_1(P) = -28.13P^{-0.295} + 34.06$$

$$f_2(P) = -11.34e^{-0.07312P} + 13.28e^{-0.4014P}$$

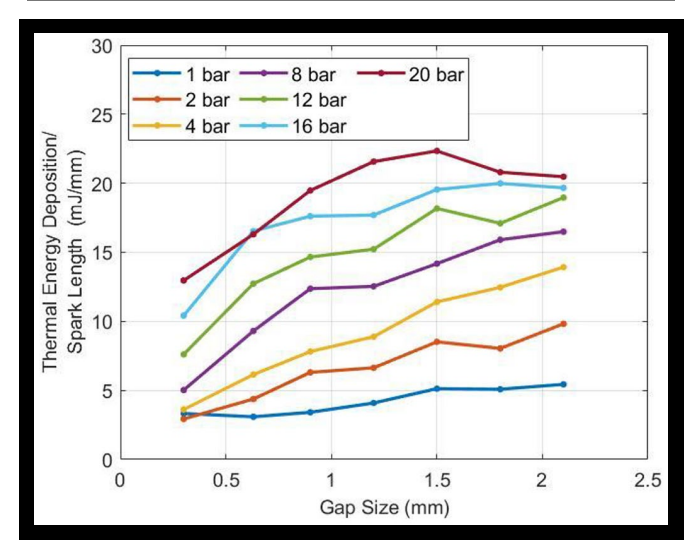
In Equation 2, d_g is the gap distance in mm and P is the gas pressure in bar, resulting in thermal energy deposition in mJ. Figure 9b shows the resulting curves from applying Equation 2 along with the data recorded from the calorimeter. The correlation shows good agreement with the data over a pressure range from 1 to 20 bar.

Figure 10 shows the energy conversion efficiency, or the percentage of the delivered electrical energy converted to thermal energy in the gas as a function of pressure and gap distance. As given in Fig. 8, the delivered electrical energy increases with both gap distance and pressure, but the even stronger increases in the thermal energy deposition lead to the strong increase in conversion efficiency with both gap distance and pressure.

Further insights into the factors affecting thermal energy deposition can be obtained through normalization of the parameters. Figure 11 shows the thermal energy deposition to the gas divided by the spark length (taken to be the gap distance, in this non-flowing gas case). It shows that the thermal energy deposited to the gas per unit length of spark, while still dependent on pressure, becomes less sensitive to gap distance for large gaps. This, presumably, is due to the diminishing relative influence of electrode heat transfer as gap distance increase.

What Fig. 11 does not take into account is the differences in delivered electrical energy to the gap for these different conditions. Figure 12 takes this into account by showing the thermal energy deposition divided by the delivered energy (conversion efficiency) per unit arc length. Here similar trends are observed, and the curves become even more flat at the larger gap distances, at least for the higher pressures.

FIGURE 11 Thermal energy deposition to the gas divided by the gap distance vs. gap distance.



This normalization, however, does not consider that the arc duration is different for all of the cases. There will be more heat transfer to the electrodes, the longer the high temperature arc is in contact with them. To account for this, Figure 13 shows the energy conversion efficiency normalized by the delivered electrical energy, arc length, and spark duration. This analysis results in a relatively flat trend at larger gaps, again suggesting the effect of heat transfer to the electrodes diminishes as the gap widens. If indeed, heat transfer losses to the electrodes are of diminished importance for large gap distances, it raises the interesting question of why the thermal energy deposition to the gas increases so strongly with pressure.

While one factor could be that at higher pressure, the lower thermal diffusivity leads to reduced conductive heat lost to the electrodes, another factor could be that the gas has a greater optical density leading to relatively lower radiation losses from the arc at high pressures. At higher optical densities

FIGURE 12 Thermal energy deposition to the gas divided by the electrical energy delivered to the gap (energy conversion efficiency) per unit length of arc vs. gap distance.

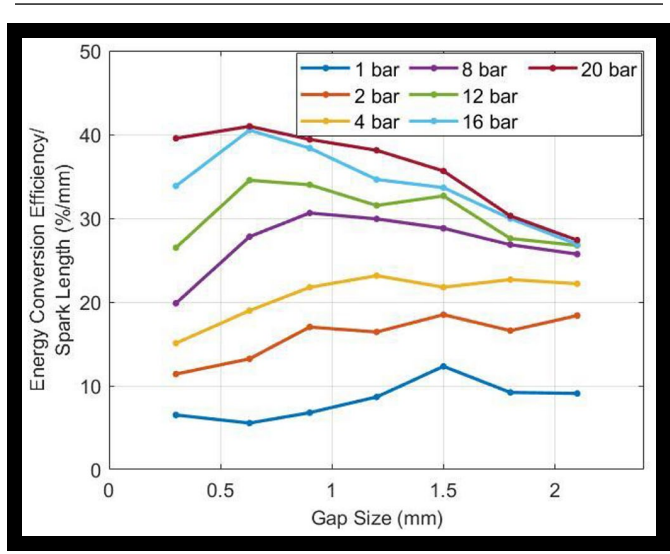
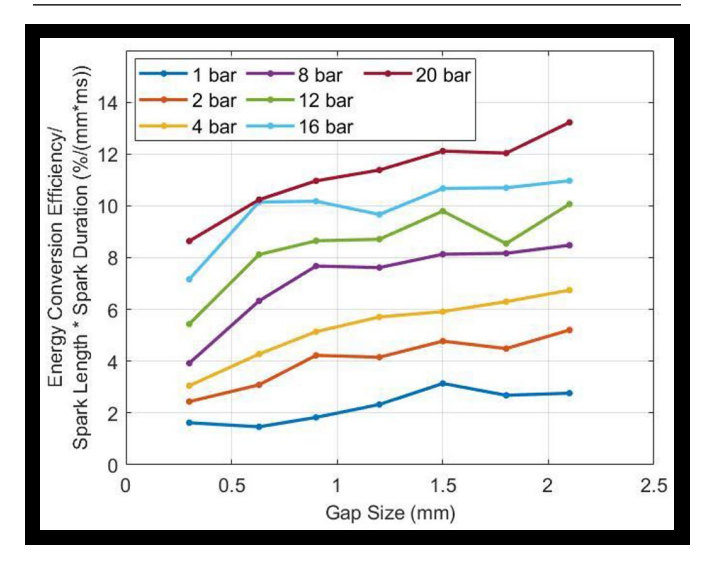


FIGURE 13 Thermal energy deposition to the gas divided by the electrical energy delivered to the gap (energy conversion efficiency) per unit length of arc divided by the spark duration vs. gap distance.



the mean free path for a photon emitted from the core of the plasma is shorter before a possible interaction and reabsorbion by another molecule, limiting the overall photon emission. Fridman and Kennedy [14] state that for high pressure arc discharges (greater than 10 atm), the thermal plasma is so dense that up to 80-90% of the discharge power can be converted to radiation.

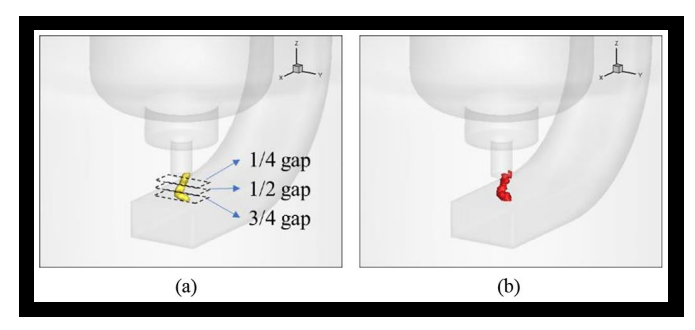
A goal of the analysis and representation was to study the possibility of using these trends to predict thermal energy deposition to the gas based on arc length for convected arcs in crossflow for which calorimeter measurements are not available. The consistency of the trends with gap size look promising but they, unfortunately, could not be validated through experiments with crossflow.

Simulation Results

The next several figures present the arc size, shape, and location for quiescent conditions from the *VizSpark* simulations. The arcs at 0.8 ms after breakdown are shown in Figure 14 (iso-surfaces of temperature in Fig. 14a and current density in Fig. 14b). The locations of three horizontal cutplanes (1/4 gap, 1/2 gap, and 3/4 gap) between the two electrodes are shown in Figure 14a. The temperature and current density fields in these planes at different times are shown in Figures 15 and 16.

The arc width or diameter was extracted from Figure 15, in which the large white circle is the periphery of the cathode; the length scale can be found to the right of the figure in units of meters. The highest temperature in the arc was above 5000 K, but would diffuse gradually in the radial direction. Due to heat flow to the surrounding gas, the affected high temperature zone was larger than the high current density zone. The current density was more concentrated within the arc and decreased with time since the gap current decreased with time

FIGURE 14 Simulation results of spark shape and location at 0.8 ms after the start of discharge, iso-surface of temperature at 2000 K (a) and iso-surface of current density at 50,000 A/m² (b), 12 bar and 0.63 mm gap



(shown in Figure 5a). The arc did not expand or narrow significantly with time, whether with respect to temperature or current density. However, the results indicated a gradual widening of the arc from 1/4 gap (near the cathode) to 3/4 gap (near the anode). Based primarily on the current density gradient, and regions where temperatures were high enough to sustain ionization of the gas, the arc diameter was estimated to be approximately 300-400 microns. The arc size and shape at the selected cutoff level of current density of $1E6 \text{ A/m}^2$ did not change much with time, and this boundary was very close to the next higher level ($2E6 \text{ A/m}^2$) boundary. In all cases, the cutoff of $1E6 \text{ A/m}^2$ corresponded to the width of 300-400 microns. The temperatures at this boundary were then examined and all were about 2500-3000 K, a temperature high enough to sustain the ionization of the gas.

The effect of pressure on the arc diameter is shown in <u>Figure 16</u>. In the 1/2 gap plane, the temperature and current density fields are compared. The arc diameter kept quite consistent, but decreased slightly with increasing pressure from 6 bar to 20 bar. The arc diameter was always very close to the cathode radius (300 microns) at the different pressures, however.

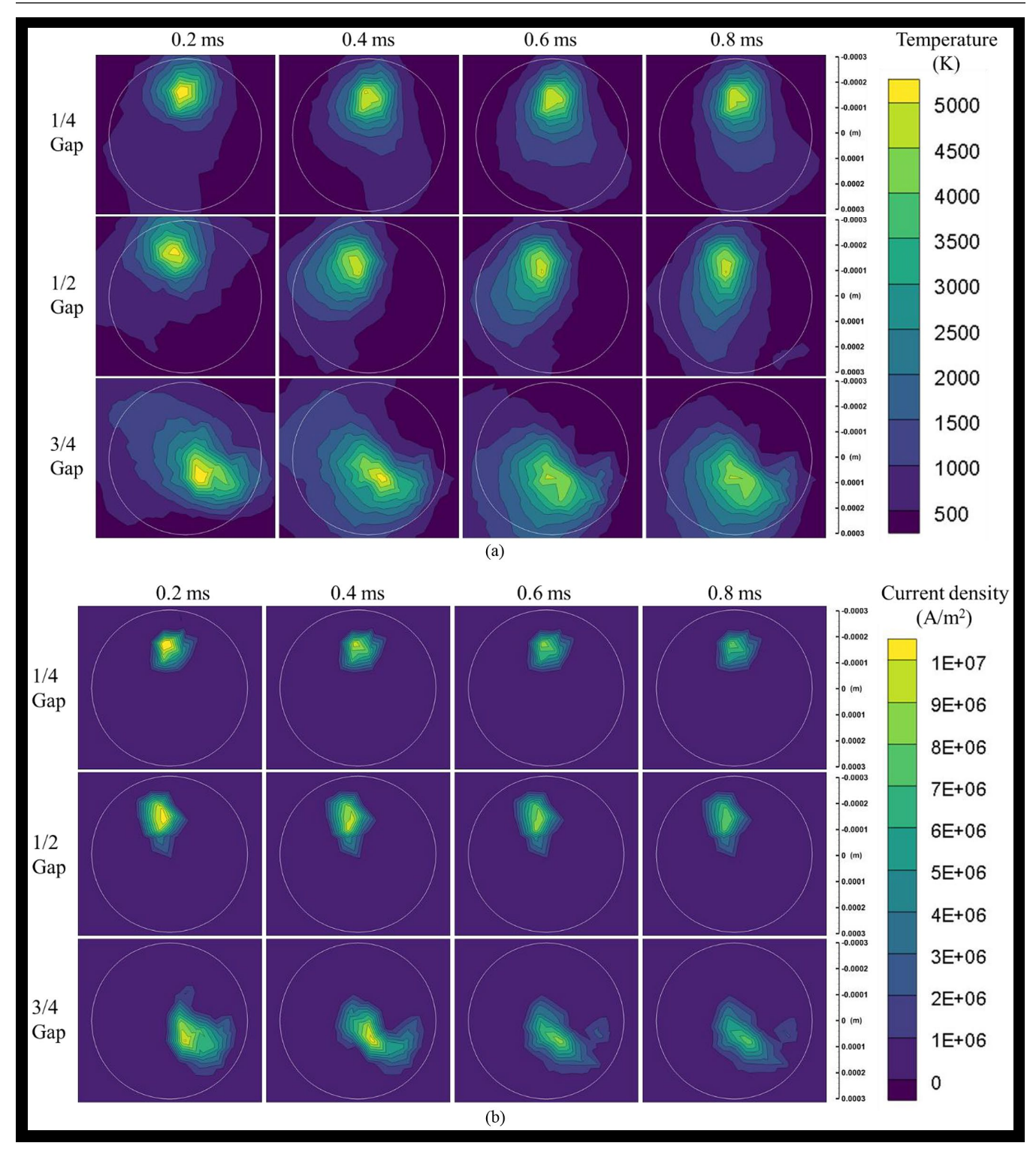
Arc Behavior and Energy Utilization for a Spark Plug in a Crossflow

Another focus of this study was the discharge characteristics of the spark plug and the ignition system energy utilization for conditions of crossflow through the gap at the higher pressures anticipated for new-generation natural gas engines. Of particular interest was the effect of crossflow velocity on breakdown voltage, arc stretch, arc width, restrike behavior, gap resistance, electrical energy delivered to the gap, spark duration, and utilization of the energy stored in the coil.

Optical Vessel

The second part of the experiments used a constant volume high-pressure vessel with optical windows for visualizing and

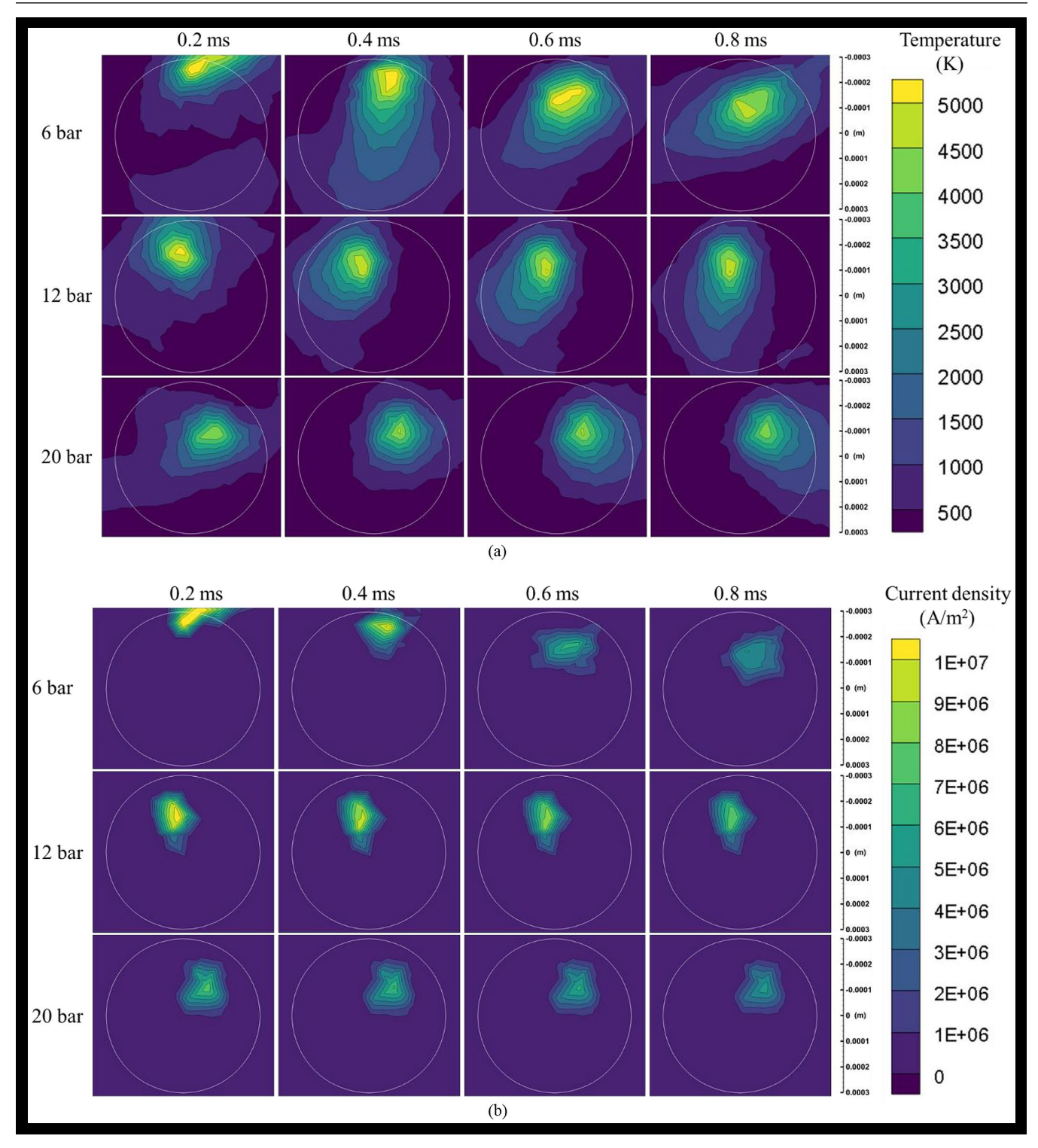
FIGURE 15 Simulation results showing the size, shape and location of the temperature field (a) and current density field (b) at different times after breakdown and at different distances between the cathode and anode, 12 bar and 0.63 mm gap.



imaging the spark. The vessel was equipped with a copper tube to inject a crossflow of nitrogen through the spark gap. A schematic of the setup is shown in Fig. 17. The vessel was cylindrical with an inner diameter of 7.9 cm and a height of 1.4 cm. The 14 mm spark plug was seated inside and positioned so that the tube would inject nitrogen perpendicular to the center electrode of the spark plug. The same high

voltage probe setup was used as in the calorimeter experiments, with the same oscilloscopes and current sensor. The flow rate of the nitrogen was measured with a rotameter located downstream of the relief valve and was calibrated using a diaphragm-type gas meter. The velocity of the gas could then be measured based on the measured flow rate and the diameter of the tube.

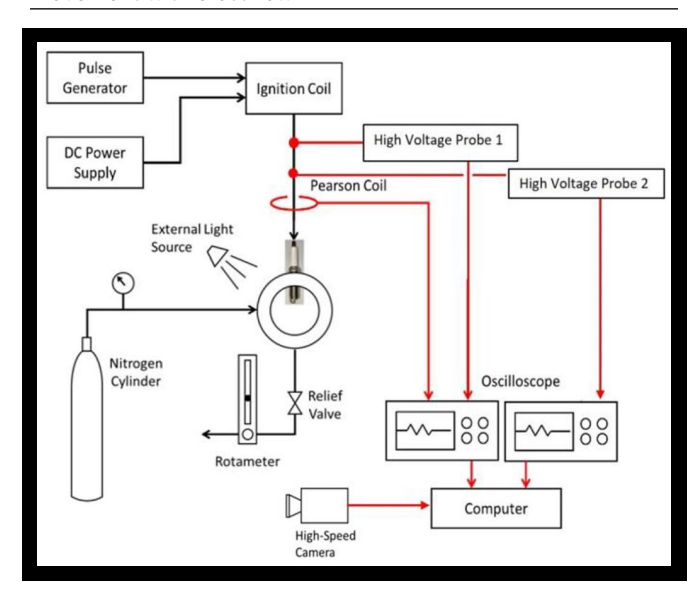
FIGURE 16 Simulation results showing the size, shape and location of the temperature field (a) and current density field (b) at different times after breakdown and at different pressures, middle cut plane and 0.63 mm gap



A Photron FastCam Mini high-speed camera was used to image the stretch of the arc due to the crossflow. It was set to record with a frame rate of 50,000 frames per second to capture the spark discharge of less than 4 ms. The frame rate was primarily limited by the maximum resolution capabilities of the camera for a given frame rate. The camera automatically cropped down the resolution of the image with an increase in frame rate due to memory limitations. Images with frame

rates above 50,000 were either too small of a field-of-view to capture the entire spark event, or too blurry from a lack of resolution due to zooming out. Therefore, 50,000 was determined as our maximum acceptable frame rate. A light source was used to illuminate the electrodes of the spark plug. After the videos were recorded, a MATLAB code was written to process the individual frames of the video and measure geometric characteristics of the arc. For these experiments,

FIGURE 17 Schematic of the high-pressure optical vessel experimental setup used for high-speed visualization of the arc movement with crossflow.



pressures were considered as high as 20 bar, with flow rates up to 30 m/s. Crossflow velocities of 30 m/s were not tested for the 20 bar case due to nitrogen flow rate limitations.

Spark gap distances used were 0.30, 0.63, and 0.90 mm. A 4 ms dwell time was used for all cases.

Experimental Results with Crossflow

<u>Figure 18</u> shows sample oscilloscope traces of the breakdown voltage with a 0.63 mm gap at pressures of 6, 12, and 20 bar, illustrating the resolution of the measurements.

The effect of crossflow velocity on the breakdown voltage is presented in Fig. 19 for three different pressures of 6, 12, and 20 bar and for gap distances of 0.30, 0.63, and 0.90 mm.

FIGURE 18 Oscilloscope trace of the breakdown voltage traces at 6 bar, 12 bar, and 20 bar with a 0.63mm gap

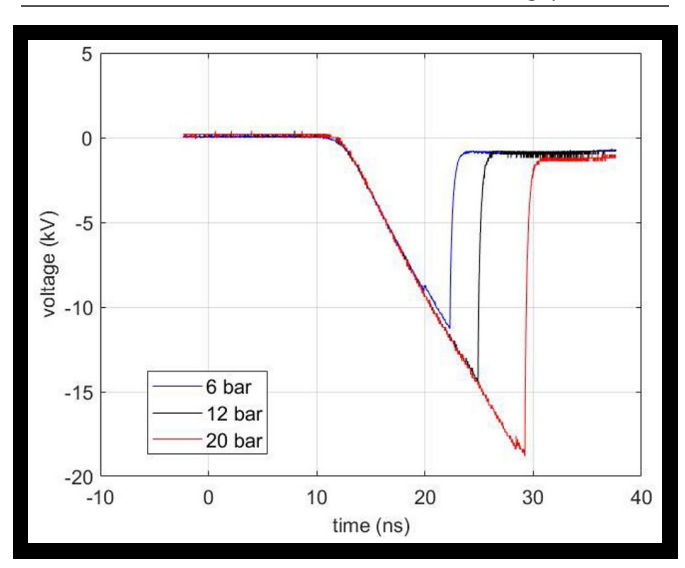


FIGURE 19 Breakdown voltage vs. crossflow velocity (a) 6 bar, (b) 12 bar, (c) 20 bar.

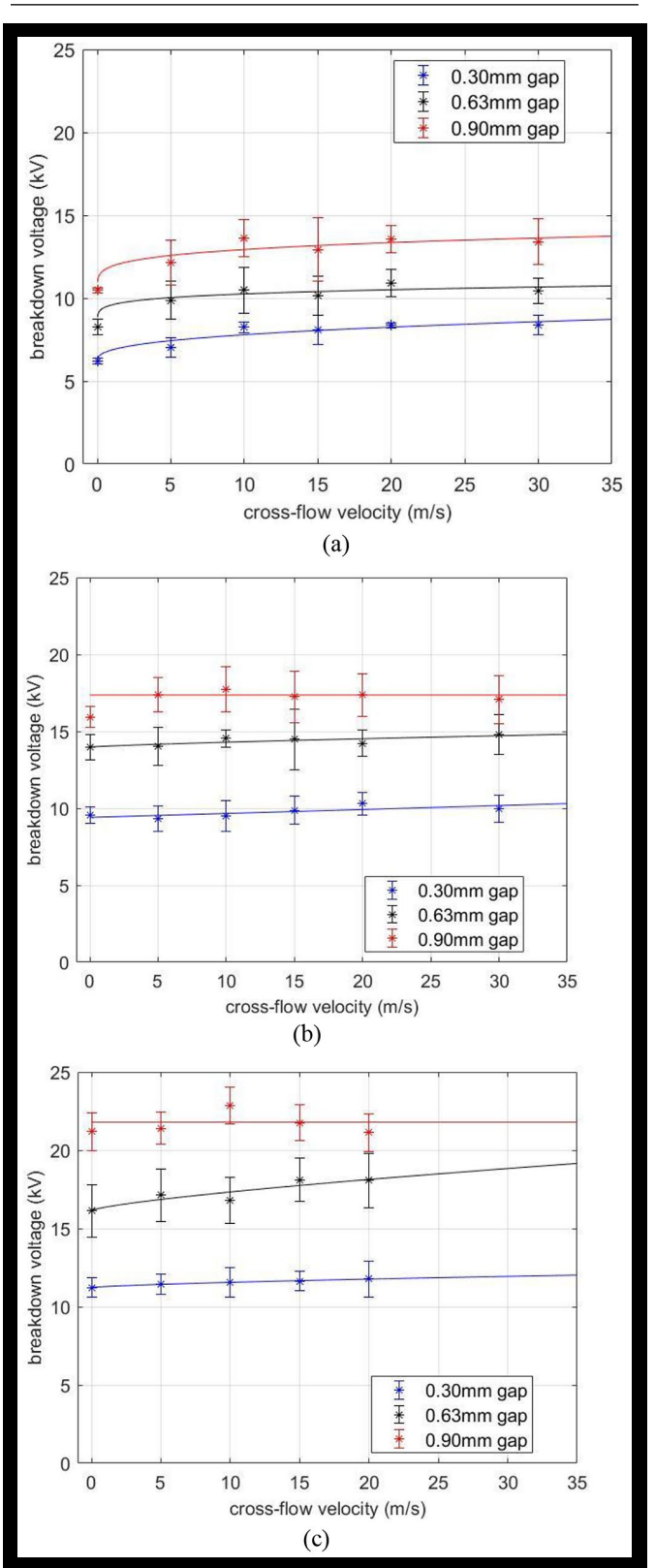
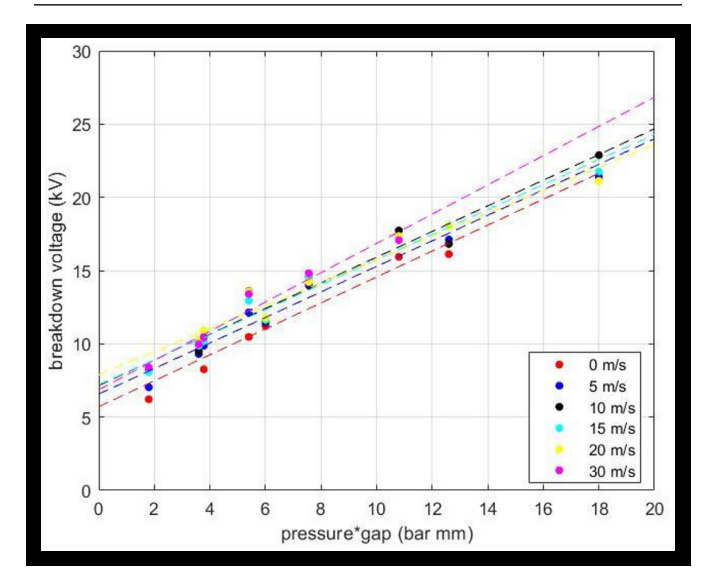


FIGURE 20 Breakdown voltage vs. pressure*gap product illustrating general adherence to Paschen's law.



The error bars represent the standard deviation of the measurements, with each data point representing an average of 10 individual trials. The results are rather unremarkable, as they indicate that breakdown voltage is almost independent of crossflow velocity. However, there does appear to be a very slight trend of increasing breakdown voltage with increasing crossflow velocity, particularly at the lowest pressure of 6 bar, comparing the no flow case with those having crossflow.

The breakdown voltage results shown in Fig. 19 can be condensed into a single graph (Fig. 20) showing the behavior in comparison to their scaling with the product of the gap distance and pressure as given by Paschen's law [15]. The data display a generally good adherence to the linear behavior predicted by Paschen's law, but the weak trend of higher breakdown voltage at higher crossflow velocities is also evident.

As mentioned in the Introduction, there have been several prior studies of restrike behavior with crossflow [2, 3, 5]. Only the study by Zadeh et al. considered crossflow at pressures as high as those examined here (up to 20 bar). Our findings were qualitatively similar to those found in prior studies; however, we considered it instructive to show some representative images of arc movement along with simultaneous measurements of discharge voltage and current, allowing visual correlation between the extent of arc movement and shape and the strike or short-circuiting event. Two examples are shown in Fig. 21 for crossflow velocities of 5 m/s (Fig. 21 a) and 15 m/s (Fig. 21b), each at a pressure 12 bar and a gap distance of 0.63 mm. The images shown in Figs. 21 and 22 are from single events recorded in the same cycle.

Whereas the follow-on arc voltage under quiescent conditions is relatively flat (Fig. 5a), with crossflow, as the arc is stretched, the negative follow-on voltage increases as the convected arc resistance increases along with its length. It is interesting that the discharge current appears to be almost completely unaffected by the convection of the arc, as it seems to be driven by the high inductance of the secondary coil that resists changes to the current passing through it. As will be discussed below, however, the crossflow velocity does indeed have an important effect on the discharge current.

Both of the image sets of <u>Fig. 21</u> show that the arc can be stretched and twisted extensively before the gap voltage reaches a level necessary for a restrike to occur. The amount of stretch at the time of restrike appears qualitatively similar for the two velocities, as are the restrike voltages, but the number of restrikes and their frequency increases as the rate of arc stretch increases with increasing crossflow velocity.

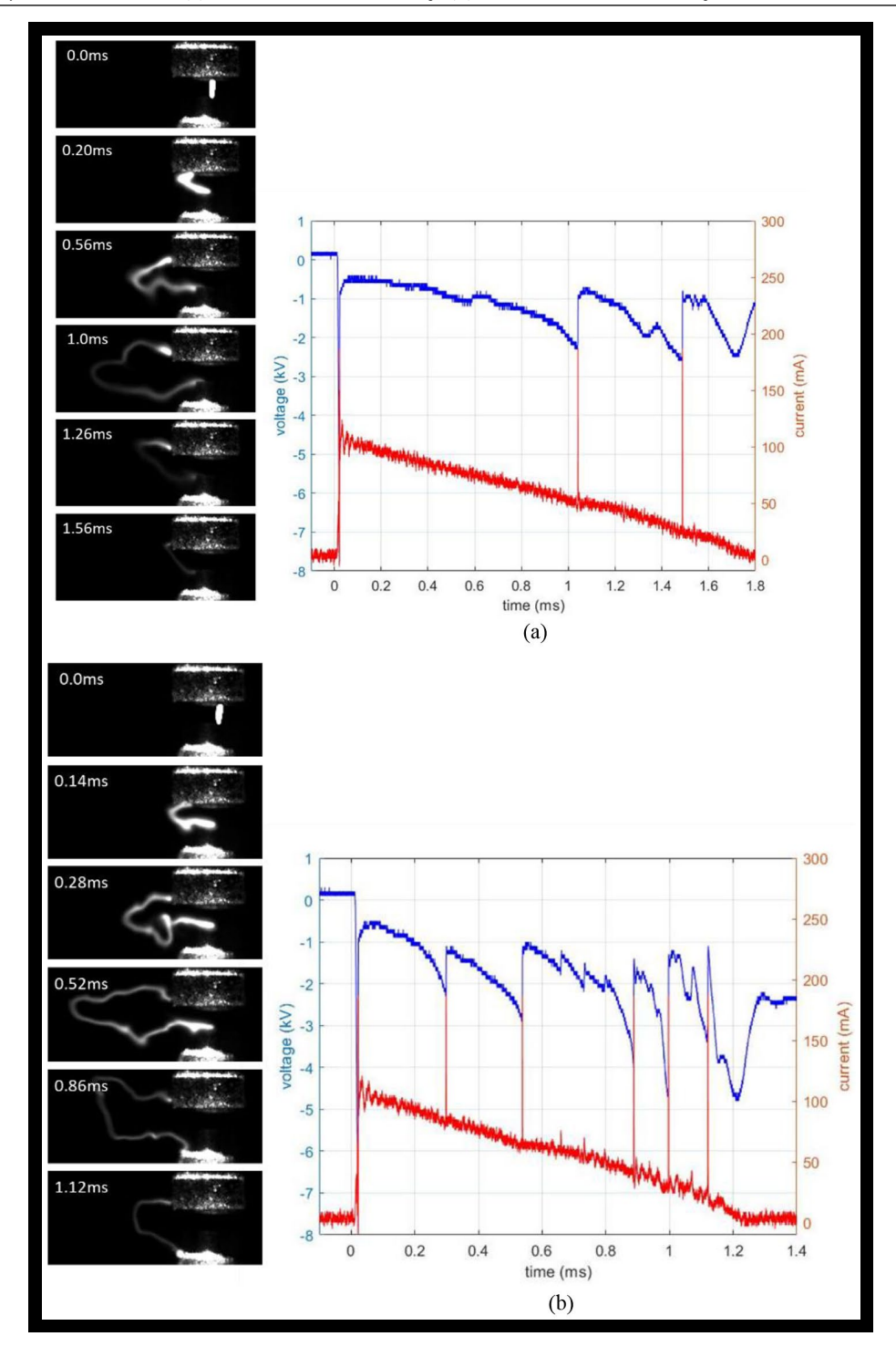
Also of interest is the effect that pressure has on arc stretch, arc width, and restrike behavior. Figure 22 shows representative images of arc stretch for the three different pressures of 6, 12, and 20 bar for a crossflow velocity of 10 m/s. The images are qualitatively similar at the three pressures; however the rate at which the arc is convected away from the gap increases with increasing pressure, presumably due to the smaller mean free path and consequent higher collision frequency between gas molecules in the flow and the electrons in the arc. Figure 22b plots the arc width for three different pressures as measured in regions of the arc that appeared stretched in the direction of the flow, as opposed to being twisted out of plane. The measured arc width was independent of pressure, with a value of approximately 300 μm, similar to that found in the VizSpark simulations. The arc width data was found following breakdown when the spark is assumed to be in the arc phase. This was done because it is very difficult to measure the arc width during the breakdown phase.

Since the time to restrike tends to decrease as the flow velocity increases, one could consider whether this easily measured metric might be used as a form of spark gap gas velocimetry. Figure 23 shows the time to first restrike as a function of crossflow velocity for three gap distances (0.30, 0.63, 0.90 mm) and for each of three pressures of 6, 12, and 20 bar. The results indicate that indeed the time to first restrike is quite sensitive to the crossflow velocity up to approximately 10 m/s, but it becomes quite insensitive to higher crossflow velocities. We also found the time to first restrike to be sensitive to the pressure at the smaller gap distances with restrikes occurring earlier at higher pressure. At the largest gap of 0.9 mm, however, the time to first restrike was less sensitive to the pressure. Based on these results, the utility of using the time to first restrike as a velocimetry tool appears limited.

Another quantity of interest is the electrical resistance of the arc as it is stretched by the crossflow and how that resistance is related to the length of the arc. This was obtained from the measured gap voltage and current along with simultaneous images for which the arc length could be measured. The electrical resistance of the stretched arc as a function of arc length is shown in Fig. 24. We developed the MATLAB-based image interrogation software used to determine arc length from the recorded images of arc stretch. Figure 24a shows the measured arc resistance as a function of the arc length using all of the data, and Figure 24b shows the same using just the first half of the data. There is considerable scatter in the data for Fig. 24a. This was due to the breakdown of the automated analysis for images recorded at later times during the discharge, caused by the faintness of the arc as the current dropped.

The luminosity of the arc gradually decreased as the discharge progressed. Beyond the point where the current fell to below approximately 1/3 its initial value following breakdown, the image dimness made it difficult for the camera to capture the darker parts of the arc, especially as

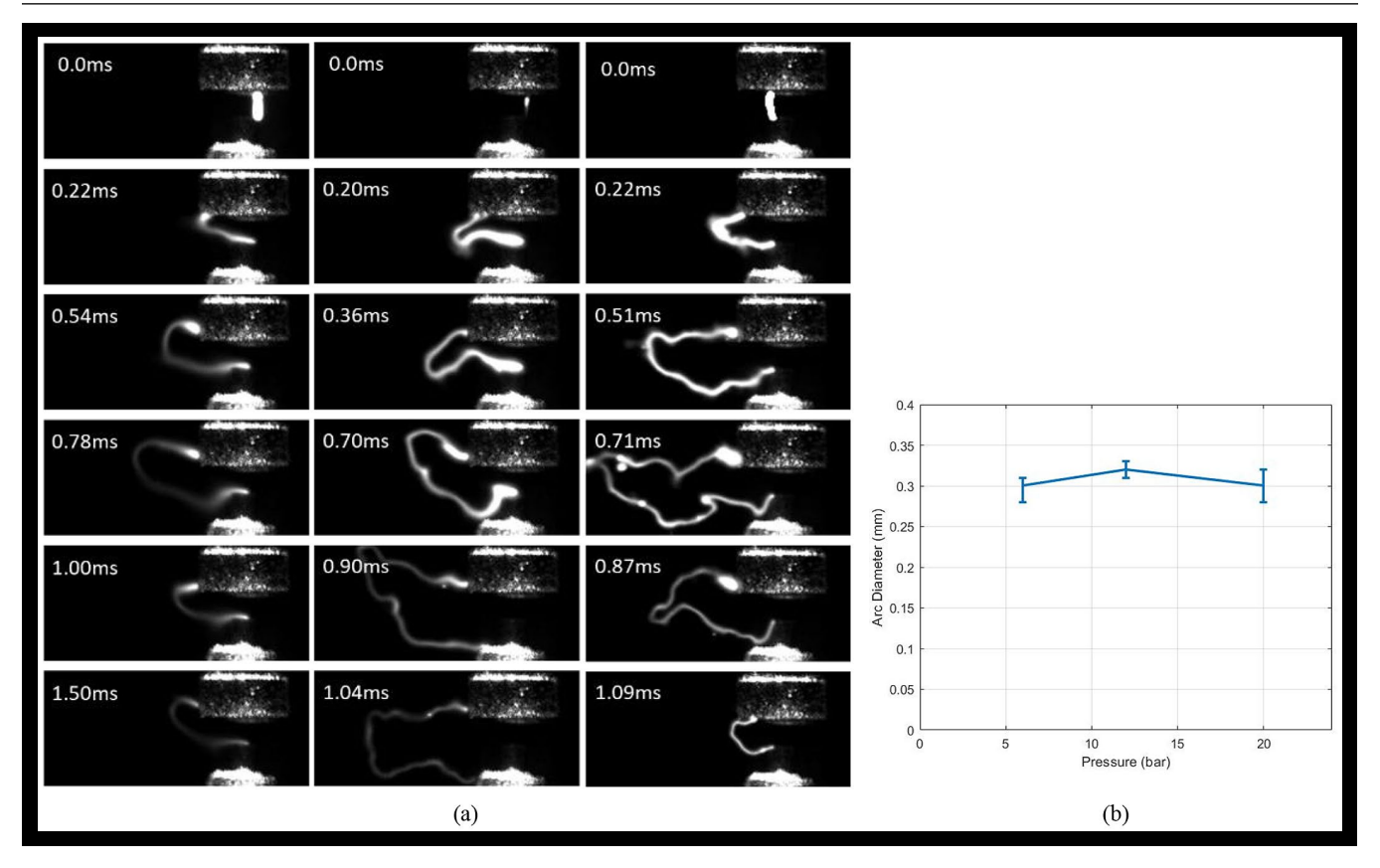
FIGURE 21 Arc movement and simultaneous current and voltage histories for a single sparking event showing correspondence with restrikes at a pressure of 12 bar, (a) 5 m/s crossflow velocity, (b) 15 m/s crossflow velocity.



the brighter spots adjacent to the electrodes overexposed the image. The result is that the MATLAB code mistook a short section of the arc for the entire thing. A better representation of the relationship between arc voltage and arc length is, therefore, given by the results shown in Fig. 24b, where only images were used from the first half of the discharge. These results show a consistent linear trend of arc resistance with length and yields a value of arc resistance per unit length of 2 kOhm/mm.

In a similar fashion, the electrical power delivered to the gap as a function of arc length was determined and is presented in Fig. 25. Again, the first figure, Fig. 25a takes the arc length from all of the recorded images and Fig. 25b, lengths from images from the first half of the discharge. As can be seen from Fig. 25b, the electrical power delivered to the gap increases approximately linearly with arc length, with a value of approximately 10W/mm. The implication of this linear dependence is that electrical power is drawn from

FIGURE 22 Arc movement at pressures of (left to right) 6 bar, 12 bar, and 20 bar with a crossflow velocity of 10 m/s (a), measured arc diameter (b).



the coil more quickly as the arc is stretched by the crossflow. Interestingly, neither the resistance per unit arc length, nor the electrical power delivery is strongly dependent on pressure.

That the electrical power delivered to the gap increases with arc length leads to the question of how the crossflow affects the total electrical energy delivered to the gap over the entire discharge duration. This is shown in Fig. 26. Figure 26 shows electrical energy delivered to the gas as a function of the crossflow velocity for pressures of 6, 12, and 20 bar (Figs. 26, a, b, and c, respectively) and parametrically as a function of gap distance.

The total electrical energy delivered to the gap increases dramatically going from the case of quiescent flow to even moderate levels of crossflow velocity, up to about 10 - 15 m/s. Above this range of crossflow velocities, the total energy delivery becomes insensitive to further increases. Another observation is that the total electrical energy delivery is sensitive to gap distance at low pressure, e.g., 6 bar, and increases with increasing gap distance. The effect of gap distance diminishes as the pressure increases. The reason for this is not clear.

From these results, an energy budget was performed to illustrate where the energy stored in the coil was going and how this is influenced by crossflow. This is shown in <u>Figs. 27a and b</u>. The energy delivered by the ignition system to the spark plug for the 4 ms dwell time was calculated based on the current-dependent inductance of the secondary side of

the coil and using $\underline{\text{Equation 3}}$. The calculated value was 155 mJ.

$$E_{sec} = \int_{0}^{i_{sec,max}} L(i) i d$$
 (3)

From this value, the energy delivered to the gap and the energy dissipated in the spark plug's internal resistor was subtracted, with the difference taken to be the un-utilized energy left on the coil.

Figure 27a parameterizes the results by pressure at various gaps and Fig. 27b parameterizes the data by gap for various pressures. Perhaps the most interesting observation from this energy budget is that energy utilization increases with increasing crossflow velocity. We did not expect this trend a priori as we envisioned that large crossflow velocities may lead to arc instabilities that could tend to extinguish the arc before all of the energy was drained from the coil. This idea was instilled by the observation that spark duration decreases as crossflow velocity increases and it was considered that hydrodynamic instabilities were driving the decrease in spark duration. On the contrary, the results suggest that the arc persists even at high crossflow velocities and is extinguished earlier for high velocities because of its more rapid power consumption and extinguishes from the depletion of energy on the coil.

Another interesting observation is that the total energy dissipated in the resistor decreases as the crossflow velocity

FIGURE 23 Time to first restrike vs. crossflow velocity at spark gaps of (a) 0.30 mm, (b) 0.63 mm, and (c) 0.90 mm

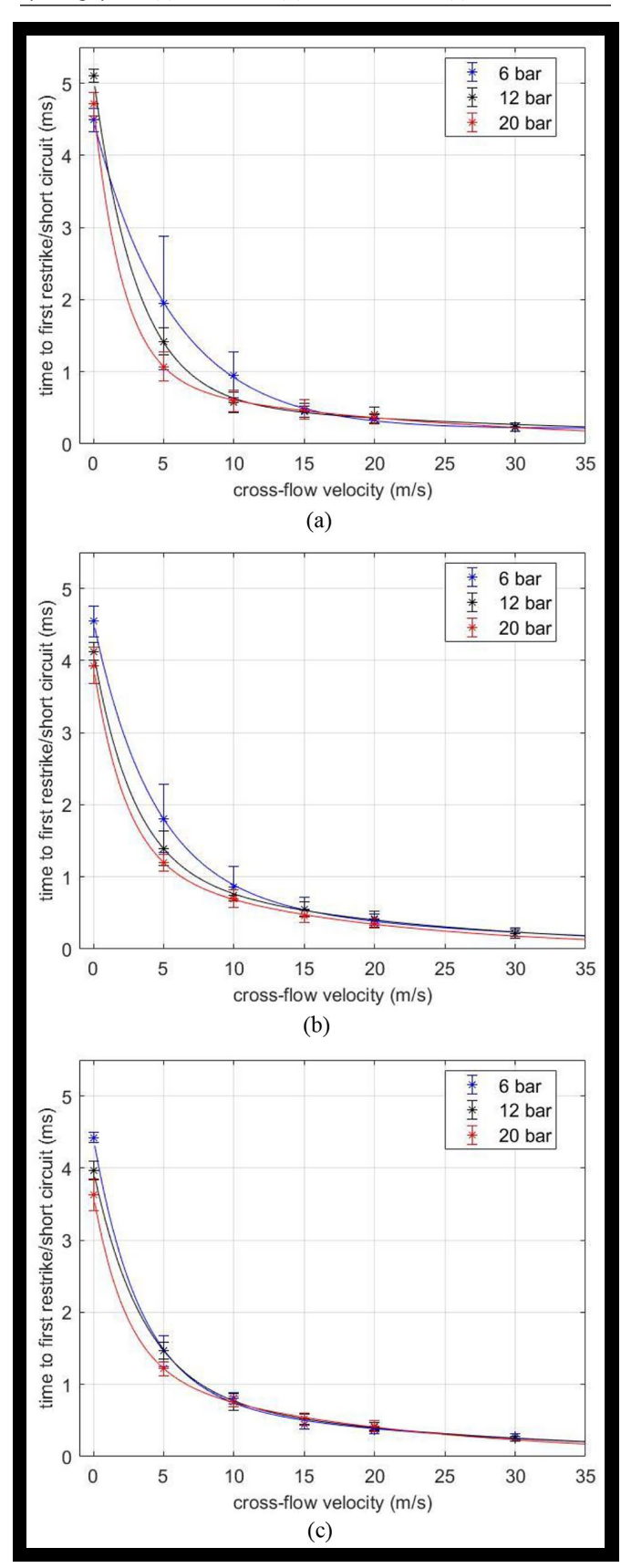
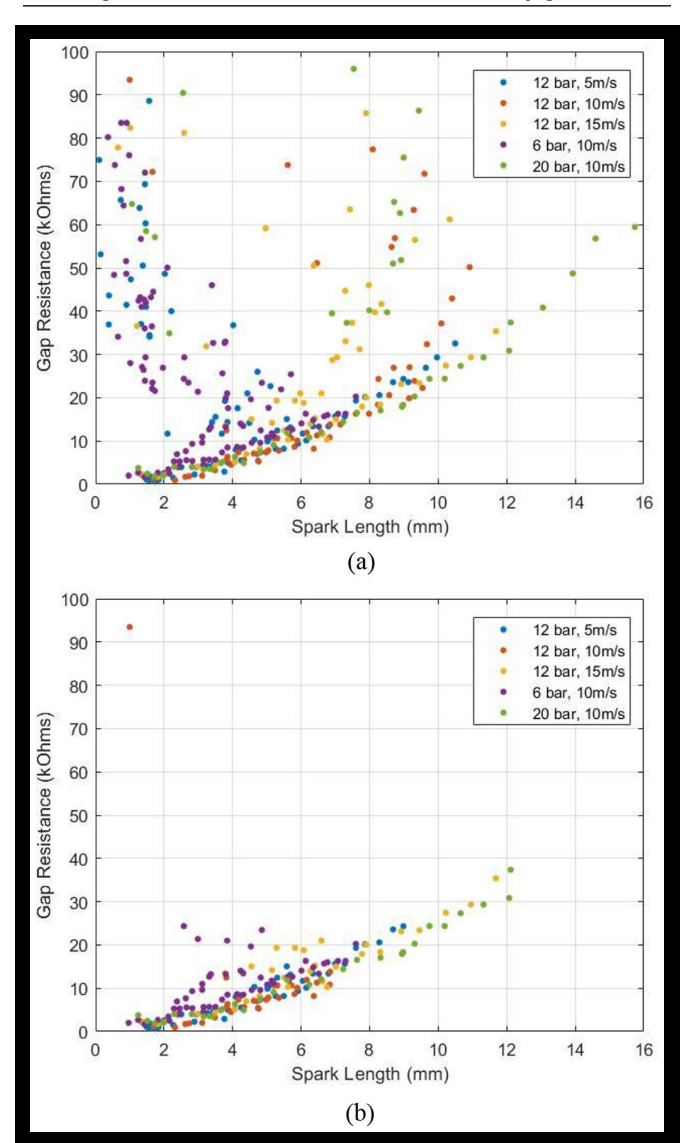


FIGURE 24 Arc resistance vs. arc length, (a) using all of the image data, (b) using only the first 50% of the data for which the image definition and contrast was consistently good.

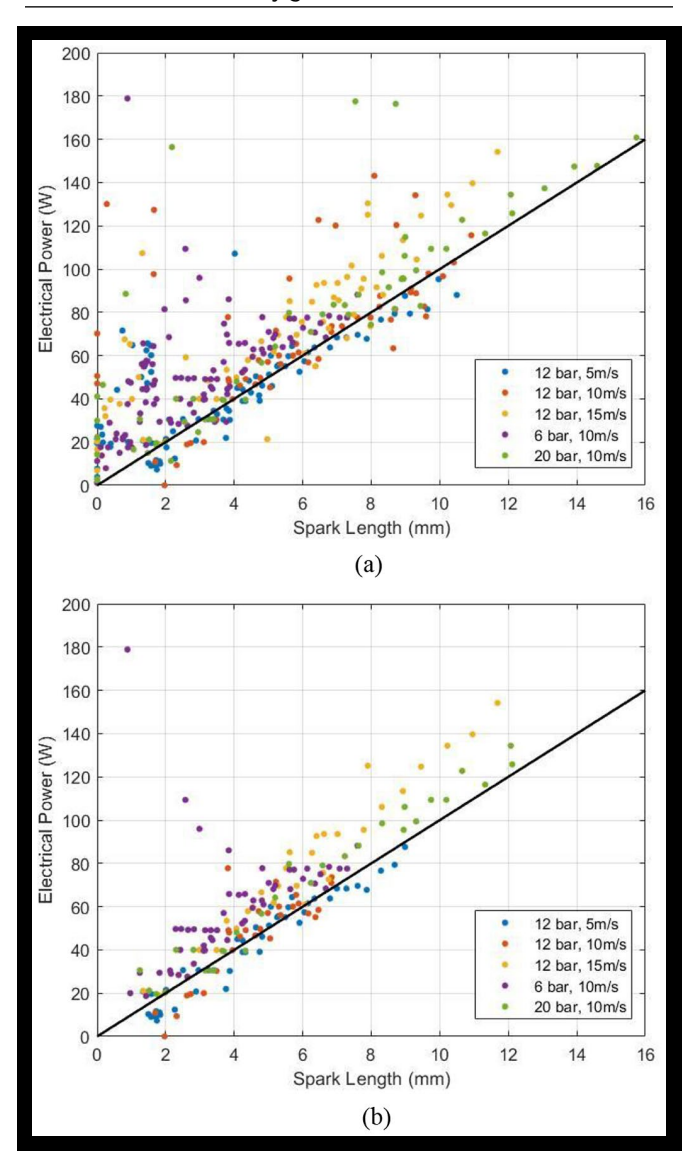


increases even though the maximum current following breakdown was approximately 100 mA for all conditions. For low crossflow velocities, the spark duration is longer, leading to more time to dissipate the current in the resistor.

These basic trends were observed for all gap distances and pressures. Figure 27a illustrates, graphically, the sensitivity of the electrical energy delivered to the gap as a function of the gap size as derived from Fig. 26. At lower pressures the delivered electrical energy increased distinctly with increasing gap size, but as noted above, the sensitivity to gap size diminished as pressure increased.

Higher pressures, however, were found to generally reduce the energy depletion from the coil. This is apparent from Fig. 27b which parameterizes the individual bars at a given crossflow velocity by pressure.

FIGURE 25 Electrical energy delivered to the spark gap vs. arc length, (a) using all of the image data, (b) using only the first 50% of the data for which the image definition and contrast was consistently good.



Summary and Conclusions

The discharge characteristics of an inductive spark ignition system were studied in quiescent conditions and with varying crossflow velocities through the gap. Under quiescent conditions the current, gap voltage, and electrical and thermal energy deposition in the gap were measured using a spark plug calorimeter for a range of pressures and spark gap distances.

Simulations of the arc size and shape for quiescent conditions were conducted with the *VizSpark* (Esgee, Inc.) multidimensional spark simulation code to validate against the experimental measurements of breakdown and follow-on voltages, current, and arc size and shape. Of particular interest was the predicted arc width (diameter) which may be important for arc-to-electrode heat transfer and for comparison

FIGURE 26 Electrical energy delivered to the spark gap vs. crossflow velocity for different gap distances, (a) 6 bar, (b) 12 bar, (c) 20 bar.

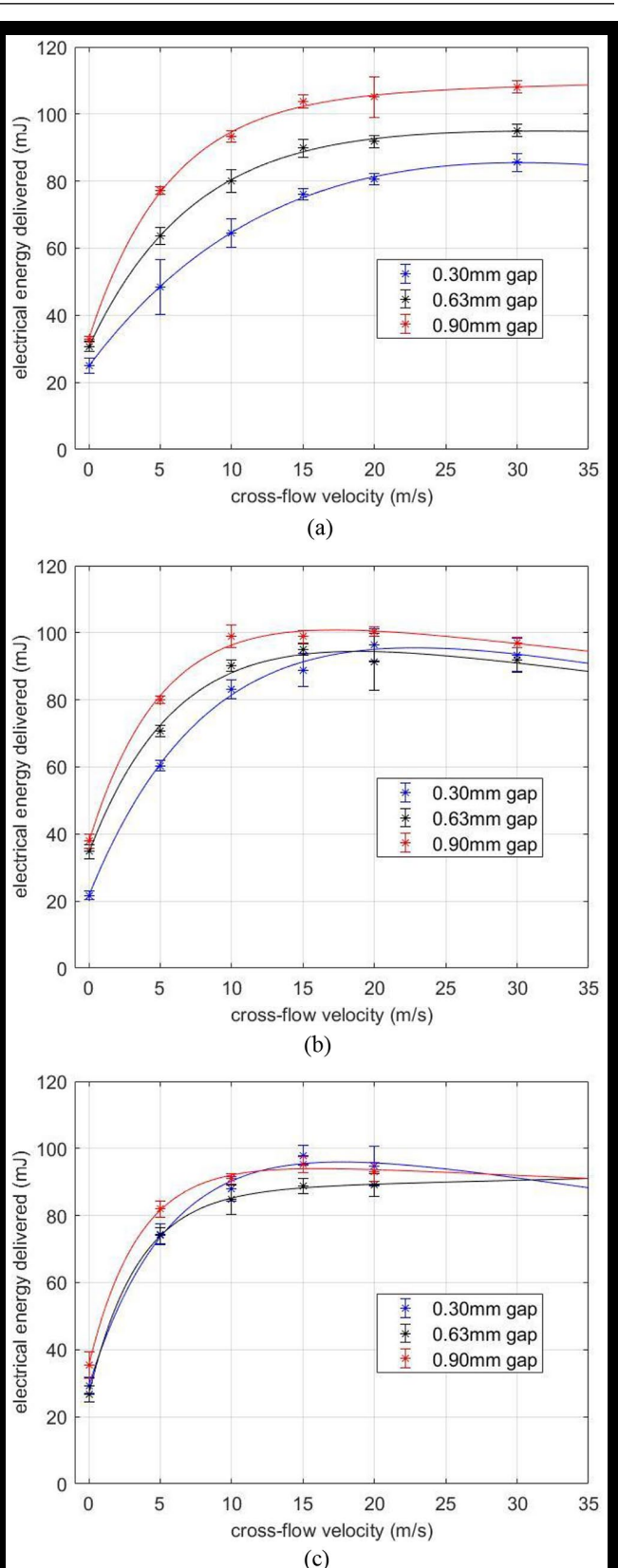
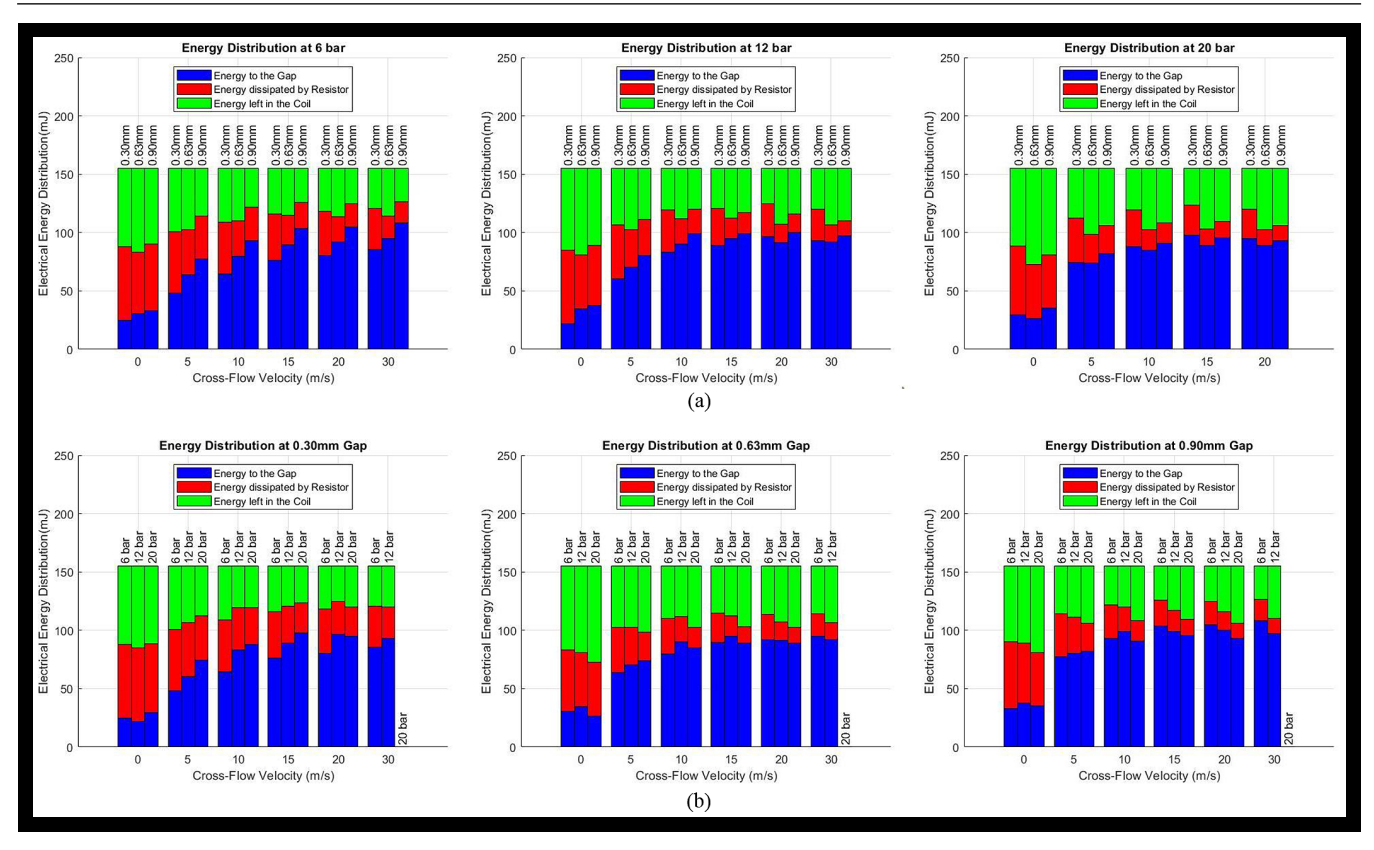


FIGURE 27 Energy utilization of the electrical energy stored in the secondary winding of the coil, including the electrical energy delivered to the gap, the energy dissipated in the spark plug internal resistor and the unused coil energy vs. crossflow velocity, (a) parameterized by pressure at various gaps, (b) parameterized by gap for various pressures.



with the measured diameter of the convected arc under crossflow conditions.

In comparison with the experiments, the *VizSpark* simulations predicted the breakdown voltage as a function of the gap distance and pressure reasonably well. The initial current and follow-on voltages were also well predicted, but both decayed more quickly than observed in the experiments resulting in a shorter predicted spark duration and delivered electrical energy.

The primary conclusions from this study were:

- 1. The simulation predicted spark width or diameter was approximately 300 400 microns as defined by the current density gradient and temperature criteria. This was similar to high-speed imaging measured values under crossflow conditions. The experimentally measured spark width was nearly independent of pressure, gap distance and crossflow velocity. The simulations predicted spark width was relatively independent of pressure up to 20 bar, but narrowed slightly with increasing pressure. The simulations also suggested a gradual widening of the arc near the anode (ground strap) relative to near the cathode (center electrode).
- 2. The calorimeter was used to measure the thermal energy deposition to the gas for gap distances wider than we have previously done, and an empirical fit

- was developed to correlate the thermal energy deposition as a function of gap distance and pressure with the hope that the trend might be extended to stretched arcs found with crossflow. This could not be verified, however, because calorimetry could not be performed in the case of crossflow.
- 3. The spark breakdown voltage was found to be largely independent of the magnitude of the crossflow velocity through the gap; however, there was a slightly increasing trend with increasing crossflow velocity
- 4. The frequency of restrikes and short circuits during discharge increased with increasing crossflow velocity. The time to the first restrike decreased with increasing flow velocity quite sharply, up to about 5 m/s velocity, but the decrease was relatively insensitive to further increases in flow velocity making it a rather poor indicator of gap velocity for anemometry predictions. The time to first restrike was also insensitive to both gap distance and pressure.
- 5. Similarly, spark duration decreased rapidly with increasing crossflow velocity up to 5 m/s, decreasing slowly with further increases in crossflow velocity. Spark duration increased with increasing gap distance and increasing pressure.

- 6. A particularly interesting finding was that the shortened spark duration caused by high crossflow velocities was due to the more rapid depletion of the electrical energy stored in the secondary side of the circuit rather than to arc instabilities associated with the disturbance of the arc by the flow. Indeed, the utilization of the energy stored in the secondary winding of the coil increased as the crossflow velocity increased and was approximately 80% utilization at high velocities, less the amount dissipated in the spark plug's internal resistor.
- 7. The gap resistance increased approximately linearly with the stretched arc length. This yielded a gap resistance of approximately 2 kOhm/mm for the stretched arcs.
- 8. The electrical power delivered to the gap also increased approximately linearly as the stretched arc length increased, with a value of about 10 W/mm of arc length.
- 9. The quantity of the electrical energy dissipated in the resistor decreased with increasing crossflow velocity due to the shorter duration of the discharge. This left a greater amount of electrical energy delivered to the gap, which tended to increase with increasing crossflow velocity.

References

- Pashley, N., Stone, R., and Roberts, G., "Ignition System Measurement Techniques and Correlations for Breakdown and Arc Voltages and Currents," SAE Technical Paper 2000-01-0245 (2000). https://doi.org/10.4271/2000-01-0245.
- 2. Shiraishi, T., Teraji, A., and Moriyoshi, Y., "The Effects of Ignition Environment and Discharge Waveform Characteristics on Spark Channel Formation and Relationship between the Discharge Parameters and the EGR Combustion Limit," *SAE Int. J. Engines* 9, no. 1 (2016). https://doi.org/10.4271/2015-01-1895.
- Yang, Z., Yu, X., Yu, S., Han, X. et al., "Effects of Spark Discharge Energy Scheduling on Flame Kernel Formation under Quiescent and Flow Conditions," SAE Technical Paper <u>2019-01-0727</u> (2019). https://doi.org/10.4271/2019-01-0727.
- 4. Maly, R. and Vogel, M., "Initiation and Propagation of Flame Fronts in Lean CH4-Air Mixtures by the Three Modes of the Ignition Spark," *17th Symposium on Combustion, the Combustion Institute* (1978): 821-831.
- Zadeh, P., M., Schmidt, H., Atkinson, W., and Naber, J., "Spark Mechanism in High Speed Flow," SAE Technical Paper 2019-01-0729, 2019, https://doi.org/10.4271/2019-01-0729.
- Huang, S., Li, T., Wang, N., Wang, X. et al., "Experimental Study on the Characteristics of Short Circuits and Restrikes of Spark Channels," SAE Technical Paper <u>2020-01-1123</u> (2020). https://doi.org/10.4271/2020-01-1123.

- Abidin, Z. and Chadwell, C., "Parametric Study and Secondary Circuit Model Calibration Using Spark Calorimeter Testing," SAE Technical Paper <u>2015-01-0778</u> (2015). https://doi.org/10.4271/2015-01-0778.
- 8. Lakshmipathi, S.M. and Deshpande, S., "Evaluation of Spark Plug Energy and Efficiency for Two Wheeler Ignition System," SAE Technical Paper 2019-26-0330 (2019). https://doi.org/10.4271/2019-26-0330.
- 9. Kim, K., Hall, M.J., Wilson, P.S., and Matthews, R.D., "Arc-Phase Spark Plug Energy Deposition Characteristics Measured Using a Spark Plug Calorimeter Based on Differential Pressure Measurement," *Energies* 13 (2020): 3550, doi:10.3390/en13143550.
- Kim, K., Tambasco, C., Hall, M., Matthews, R. et al., "Multi-Dimensional Spark Ignition Model with Distributed Energy Input and Integrated Circuit Model," SAE Technical Paper 2021-01-0405 (2021). https://doi.org/10.4271/2021-01-0405.
- 11. Kim, K., Tambasco, C., Hall, M., and Matthews, R., "Experimental and Modeling Study of Spark Plug Electrode Heat Transfer and Thermal Energy Deposition," SAE Technical Paper 2021-01-0480 (2021). https://doi. org/10.4271/2021-01-0480.
- Breden, D.P., Karpatne, A., and Raja, L., "Modelling of Electrode Erosion for Prediction of Spark Plug Lifetime," SAE Technical Paper <u>2018-01-0175</u> (2018). https://doi.org/10.4271/2018-01-0175.
- 13. Subramaniam, V., Karpatne, A., Breden, D., and Raja, L., "Simulation of Spark-Initiated Combustion," SAE Technical Paper 2019-01-0226 (2019). https://doi.org/10.4271/2019-01-0226.
- Fridman, A. and Kennedy, L.A., *Plasma Physics and Engineering*, Ch. 8, Taylor and Francis Pub., New York, 2004.
- Meek, N.F., Electrical Breakdown of Gases (London, UK: Oxford at the Clarendon Press, 1953)

Contact Information

Prof. Matthew J. Hall

mjhall@mail.utexas.edu
The University of Texas at Austin
Department of Mechanical Engineering
204 E. Dean Keeton St. C2200
Austin, TX 78712

Acknowledgments

This project was made possible through funding provided by Cummins Inc. through the University of Texas at Austin's site of the NSF Center for Efficient Vehicles and Sustainable Transportation Systems (EVSTS). The authors wish to express their gratitude to Sachin Joshi, Daniel J. O'Connor and Douglas L. Sprunger of Cummins Inc. for many helpful discussions.

We wish to thank Esgee Technologies for providing us with licenses for their simulation software and for their generous technical support. The Texas Advanced Computing Center (TACC) of the University of Texas at Austin provided the computational resources for the simulations. Those simulations would not have been possible without their continued support.

^{© 2021} SAE International. All rights reserved. No part of this publication may be reproduced, stored in a retrieval system, or transmitted, in any form or by any means, electronic, mechanical, photocopying, recording, or otherwise, without the prior written permission of SAE International.